JOURNAL OF MATERIALS SCIENCE 33 (1998) 395–403

The effect of tempering temperature on mechanical properties and microstructure of low alloy Cr and CrMo steel

M. GOJIĆ
Iron Steel and Works Sisak, Sector for Development, B. Adžije 2, Sisak, Croatia

L. KOSEC
Faculty of Natural Sciences and Engineering, Department of Materials and Metallurgy, Aškerčeva 12, Ljubljana, Slovenia

P. MATKOVIĆ
Faculty of Metallurgy Sisak, University of Zagreb, Aleja narodnih heroja 3 Sisak, Croatia

Two low alloy Cr and CrMo steels with similar levels of carbon, manganese and chromium have been studied to determine the effect of tempering temperature on the mechanical properties and microstructure. The quenching and tempering of steels were carried out using a high-speed dilatometer. The steels were quenched at the average cooling rate of 30 K s^{-1} in the temperature range from 1123 to 573 K by flowing argon and tempered at 673, 823 and 973 K. The martensite of steels formed during quenching was of entire lath morphology with 2 vol% retained austenite. It was found that after tempering at 973 K the Cr steel contained only orthorhombic cementite, while the CrMo steel contained the cementite and hexagonal Mo_2C particles in the ferrite matrix. At the same tempering conditions, the CrMo steel shows higher strength but lower ductility as compared to those of Cr steel. It is shown that this difference results from finer prior austenite grain, substructure within matrix and precipitate dispersion strengthening, primarily by Mo_2C. Transmission electron microscopy (TEM) bright- and dark-field micrographs as well as selected area diffraction pattern analysis of orientation relationship showed that the cementite precipitated from the ferrite matrix. Fractography analysis showed that the morphology fracture surface was changed by increasing tempering temperature. Tempering at 973 K obtained ductile fracture by the microvoid coalescence mechanism.

1. Introduction

High-strength low alloy Cr and CrMo steels have generally been used as structural components in power generation, chemical, oil and petrochemical industry [1, 2]. The main reason for these applications is in their excellent hardenability, high strength, good toughness and high resistance to corrosion. A typical heat treatment for these steels involves quenching and tempering. Considerable research effort has been directed to determine the relationship between the microstructure and mechanical properties in high strength low alloy steels as the result of heat treatment [3, 4]. Although significant advances have been made in unravelling the process underlying the tempering behaviour, a complete and satisfactory understanding of the mechanisms of the structural changes involved has not yet been obtained. It is known that this process leads to the formation of a homogeneous microstructure consisting of ferrite and precipitates. However, the results published in literature showed that the precipitates in the matrix caused by the heat treatment are different. At equilibrium the carbide sequence in the Fe–Mo–C system with the increasing Mo : C ratio is following: Fe_3C, $M_{23}C_6$($Fe_{21}Mo_2C$), Fe_2MoC, M_2C and M_6C [5]. Baker and Nutting [6] were the first who investigated systematically the sequence of carbide precipitation during tempering of 2.25Cr–1Mo steel. By tempering at 953 K for 6 h they obtained Fe_3C, Mo_2C and Cr_7C_3 in the ferrite matrix. Murphy and Branch [7] studied normalized and tempered 2.25Cr–1Mo steel and found evidence of M_3C and M_2C with an occasional presence of $M_{23}C_6$. Pilling and Ridley [8] also observed the rodlike precipitates and indicated that they could be either $M_{23}C_6$ or M_6C. Bišs and Wada [9] observed that the carbides in the 1Cr–0.5 Mo steel are cementite and Mo_2C particles, while Craig observed Fe_2MoC carbides in CrMo steel for tempering temperature above 923 K [10].

Since the effect of quench rate on the mechanical properties of steels having martensite microstructure is well defined [11, 12], it is necessary to quench steels at constant cooling rate in order to obtain the same base for tempering. Due to the well defined

0022–2461

conditions it is possible to obtain the base using heat treatment by dilatometry method. The low alloy Cr and CrMo steels were chosen for consideration in this test programme. The steels have the same composition except molybdenum content. In this work the mechanical properties and microstructure of quenched and tempered steel vary by tempering at 673, 823 and 973 K. The effect of tempering temperature on mechanical properties and microstructure of steels was investigated by using series microstructural techniques. In order to obtain the complete state of the effect of tempering and microstructure on fracture in these two steels, fractography tests were performed.

2. Experimental procedure

2.1. Material and heat treatment

The low alloy Cr and CrMo steels were prepared by melting in an induction furnace and casting in ingots. The ingots were hot rolled to tube using normal industrial conditions. The chemical composition of steels is given in Table I. Cylindrical specimens 4.8 mm in diameter and 30 mm length were cut from the tubing parallel to the rolling direction. The heat treatment (quenching and tempering) of specimens was carried out using a high-speed dilatometer. The temperature level, heating rate and duration at the level in seconds were chosen on the programmer. When the programmer was linked to the temperature controller, the furnace was subjected to the desired heating programmes. Two thermocouple wires are welded on the gauge length of specimen using welder supplied with the dilatometer. Temperature sensing was performed by a chromel/alumel thermocouple (73 to 1643 K) linked to a temperature amplifier, and then to the x-axis of the recorder. The temperature was controlled by means of a linear heating programme. The set voltage was compared to the voltage transmitted by the measurements thermocouple. The difference between the two voltages was applied to a high-gain amplifier which controls the intensity of the heating current of the furnace so that, at any moment, the difference between the voltage and the thermocouple voltage was close to zero. For a given specimen the hold temperature, heating rate and cooling rate were uniform over the gauge length. Heat from radiation furnace was radiated by two tubular quartz lamps with tungsten filaments at the focal point of a double elliptical polished aluminium reflector, and was focused on the gauge length of specimen centred on a common focal axis. During the heat treatment the specimens were protected from oxidation by vacuum of 0.13332 Pa. The specimens were heated with the heating rate of $0.5\,K\,s^{-1}$ up to 1123 K and austenitized for 600 s. Quenching was performed by blowing argon through a perforated tube into the sealed chamber and over entire gauge length. The average cooling rate was measured using the suitable openings of the argon inlet valve, time base of recorder and timer which automatically marks time above the cooling curve from austenitizing temperature (1123 K) to 573 K. To eliminate the diffusion-controlled transformations the average rate of $30\,K\,s^{-1}$ in the temperature range from 1123 to 573 K was used. Immediately after quenching the specimens were tempered in range temperature from 673 to 973 K for 2400 s, followed by air cooling.

TABLE I Chemical composition of steels investigated, wt %

Steel	C	Si	Mn	P	S	Cr	Mo	Al	Cu	V
Cr	0.44	0.38	0.80	0.017	0.027	1.11	0.11	0.04	0.08	0.01
CrMo	0.41	0.26	0.87	0.015	0.020	1.01	0.70	0.04	0.06	0.01

2.2. Mechanical properties and metallography

After heat treatment the specimens were used for tensile testing. Mechanical properties were determined using an Instron tensile machine type 1196 at strain rate of $2.5 \times 10^{-5}\,s^{-1}$. Hardness measurements were made using a Vicker's pyramid hardness tester and a load of 30 kg.

The microstructure of steel was studied using optical microscopy (OM), scanning electron microscopy (SEM), X-ray diffraction (XRD) and transmission electron microscopy (TEM). Samples for OM and SEM were polished mechanically to 1000 grit with SiC papers, then with 0.5 μm alumina powder, to obtain a mirror surface. The prior austenite grain boundaries of steels were revealed with etchant developed by Enomoto *et al.* [13]. Samples for the SEM were etched in nital solution. Microstructural examination was by SEM, operated at 50 kV. Fractography was performed using SEM on fresh fracture surfaces from the tensile specimens broken at room temperature.

Thin foils for TEM were obtained by mechanical grinding to 0.2 mm thickness and then by chemical thinning in a mixed solution of hydrofluoric acid and hydrogen peroxide. The foils were electrolytically etched for 3 h. Subsequently foils were examined by TEM Jeol JEM 2000FX operated at 200 kV equipped with a facility for energy dispersive X-ray spectrometry (EDXS).

The retained austenite content was measured by X-ray diffraction using Miller's technique of rotating and tilting the specimen surface about an incident beam CoK_α radiation. The combination of (2 1 1)α, (2 2 0) γ and (3 1 1) γ peaks was chosen for the analysis.

The phase identification of steel samples tempered at 973 K was performed by XRD method using a counting technique with the application of CuK_α radiation. The obtained diffractographs were analysed by the comparison method with the use of JCPDS data [14].

3. Results and discussion

3.1. Mechanical properties and microstructure of steels in rolled condition

Mechanical properties of steels in rolled condition are shown in Table II. The mechanical properties reported are the average of three determinations. The

TABLE II Mechanical properties of low alloy Cr and CrMo steel in rolled condition

Steel	Yield strength (MPa)	Tensile strength (MPa)	Reduction of Area (%)	Hardness ($H_{V_{30}}$)
Cr	962	1110	15	375
CrMo	1103	1236	12	399

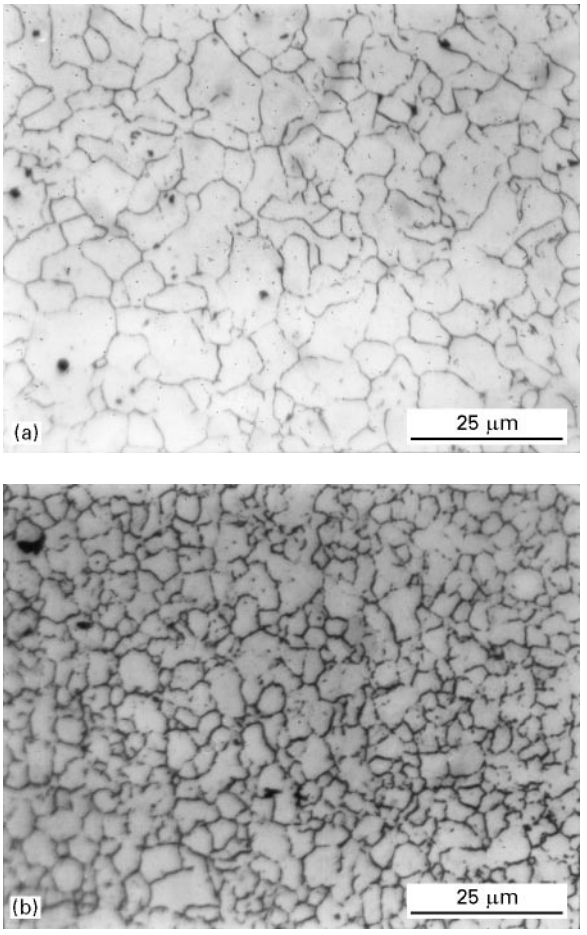

Figure 1 Prior austenite grain boundaries of steels investigated: (a) low alloy Cr Steel, (b) low alloy CrMo steel.

value of mechanical properties and hardness were reproducible within 2%. Tensile strength and hardness of CrMo steel were 10% higher than those of Cr steel. It is due to the beneficial effect of molybdenum which improves hardenability of steel and decreases prior austenite grain size [15, 16]. Fig. 1 shows prior austenite grains of Cr and CrMo steel. As can be seen, the CrMo steel has a fine austenite grain size corresponding to an ASTM grain size of 12 (7 μm average grain size), while the Cr steel has a coarser grain size corresponding to an ASTM grain size of 10 (14 μm average grain size).

The high values of mechanical properties of steels in rolled condition resulted from the bainite microstructure obtained by continuous cooling with finish rolling temperature of 1153 K. It is known that the bainite is the most complicated microstructure of steel and it represents a mixture of ferrite and cementite [17]. Based on studies of the morphology of bainite, Habraken *et al.* [18] have proposed that the bainite formed during continuous cooling of CrMo steel is very different from that expected during isothermal transformation and hence has been termed as "non-classical bainite". The mechanism of bainite formation, which in turn influences its morphology, depends strongly on the rate of cooling in the temperature range from 1023 to 773 K. Accordingly, the continuous-cooling transformation (CCT) diagram is divided into three regions: formation of carbide-free acicular bainite; "granular" bainite consisting of ferrite with high dislocations density which contains martensite–austenite islands and a mixture of polygonal ferrite and bainite, which is sometimes referred to as "pseudo pearlite" [19]. Microstructure of Cr steel shown in Fig. 2a corresponds to the microstructure described as "pseudo pearlite" because of its lamellar

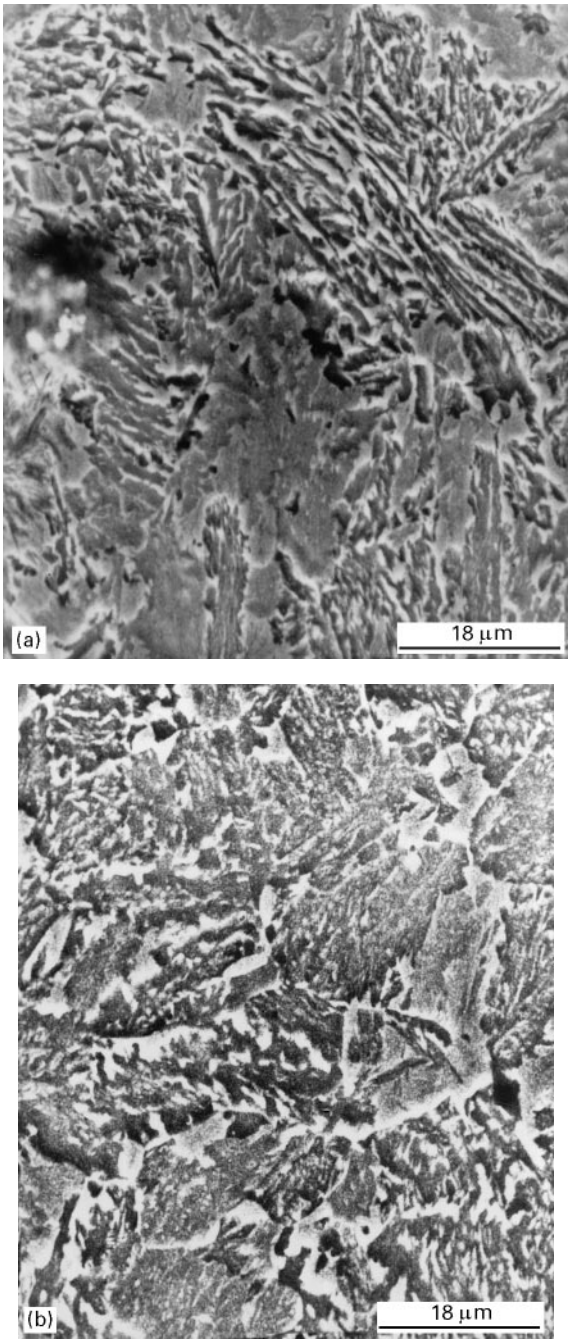

Figure 2 Scanning electron micrographs of low alloy Cr (a) and CrMo (b) steel in the rolled state.

appearance. In 2.25Cr–1Mo steel this microstructure has often been improperly identified as pearlite [20]; in another work this lamellar product was shown to be bainite because of the temperature range in which it had been formed [21]. However, the SEM micrograph of CrMo steel (Fig. 2b) revealed that the bainite microstructure was composed of packets which consisted of ferrite laths separated by regions of martensite or cementite or austenite in a prior austenite grain, but no clear regions of blocks were delineated by the present etching procedure. Taking into consideration the hardness of steels in Table II (374 and 399 HV_{30} for Cr and CrMo steel, respectively) the bainite corresponds to the cooling curves passing through the ferrite-pearlite-bainite range of CrMo steel CCT diagram [22].

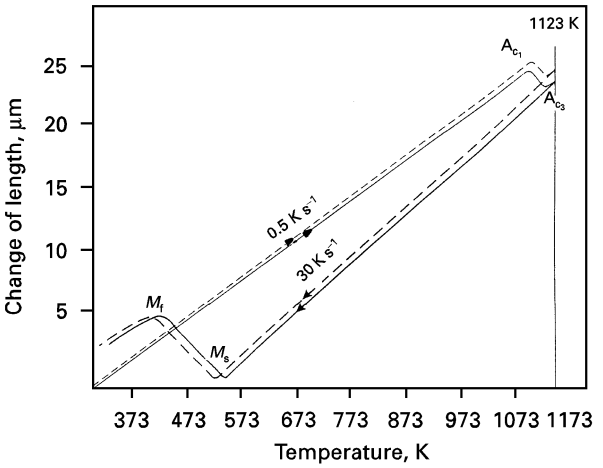

Figure 3 Dilatometric curves on heating and cooling of low alloy Cr (—) and CrMo (- - - -) steel. Heating up to 1123 K and cooling to room temperature was performed under vacuum at rates of 0.5 K s^{-1}. Ac_1, Ac_3, M_s and M_f corresponding to the points of inflection on the curves of heating and cooling.

3.2. Microstructure and mechanical properties of steels after heat treatment

Fig. 3 represents dilatometric heating and cooling curves of steels. Heating of steels up to 1123 K was accompanied by contraction in the temperature range from 1023 (Ac_1) to 1063 K (Ac_3) for the Cr and from 1033 (Ac_1) to 1083 K (Ac_3) for the CrMo steel, respectively. It corresponds to the change of the body centred cubic (α-Fe) into the face centred cubic lattice (γ-Fe). After austenitizing at 1123 K for 600 s the steel was quenched by flowing argon at the average cooling rate of 30 K s^{-1} in the temperature range from 1123 to 573 K. Because of a high cooling rate and hardenability of steel, the diffusion-controlled transformations at high temperatures (ferrite, pearlite and bainite) did not appear, then only martensite occurred. On the cooling curve, start (M_s) and finish (M_f) temperatures of martensite were located. The formation of the martensite (at 513 and 503 K for Cr and CrMo steel, respectively) was accompanied by increasing dilatation and probably it was formed by a shear mechanism [23]. During further cooling below M_s temperature there was very little carbon diffusion and the austenite was transformed mainly to martensite at M_f (at 413 and 403 K for Cr and CrMo steel, respectively). Although the bulk M_s and M_f temperatures of steels were above room temperature (dilatometry cooling curves, Fig. 3) the X-ray diffraction analysis revealed some amounts (2 vol%) of retained austenite. This phase may be in the form of a very thin and continuous film between the martensite laths [24]. The existence of retained austenite at room temperature in these steels may be attributed to the high carbon content of the austenite [25]. The formation of martensite is by diffusionless

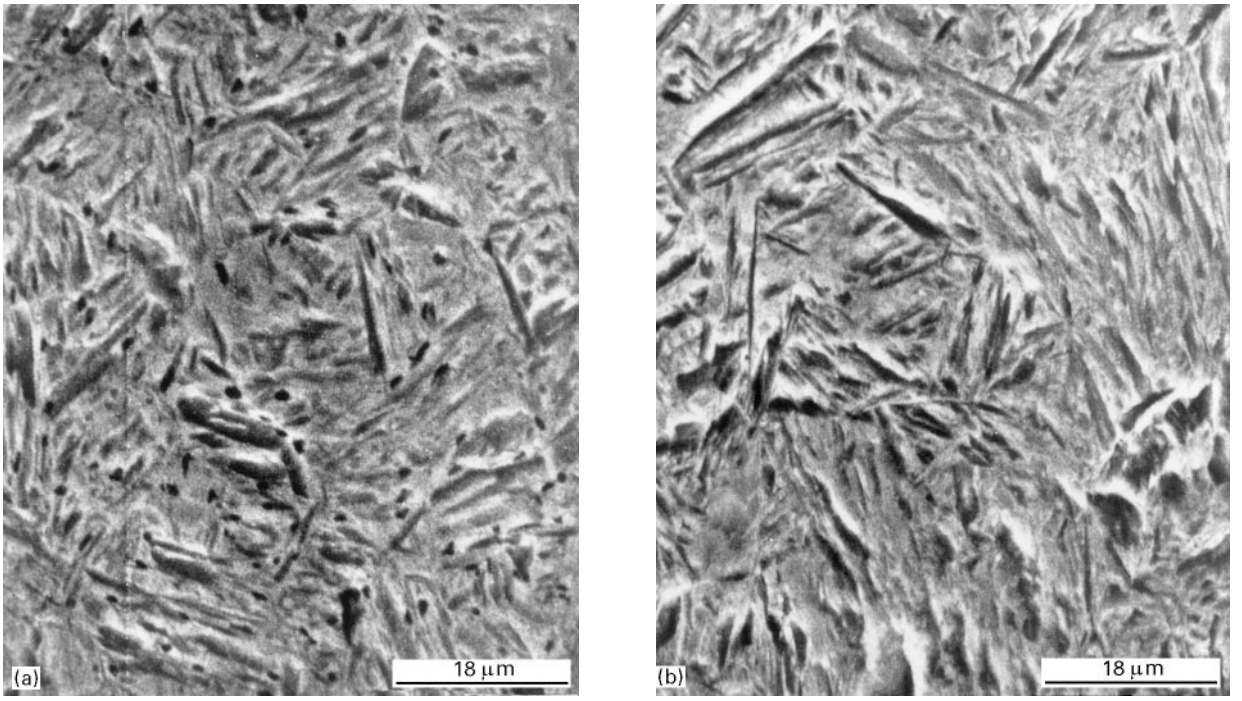

Figure 4 Scanning electron micrographs of low alloy Cr (a) and CrMo (b) steel austenized at 1123 K and quenched by flowing argon at the cooling rate of 30 K s^{-1}.

transformation, which was accompanied by the volume expansion, thus a certain austenite content may be retained between martensite laths. Scanning electron microscopy analysis showed that there were no major differences in the microstructure of steels after quenching (Fig. 4). The microstructures are composed of martensite packets containing laths. As can be seen from the SEM micrographs the basic units are martensite laths aligned parallel in packets within austenite grain. Detailed characterization of CrMo steel in the quenched state by TEM confirmed that the morphology of martensite is basically dislocated lath type (Fig. 5). The structure of lath martensite can be characterized by its substructure of tangled dislocations within laths. The width of laths which make up packets of martensite is from 0.5 to 1 μm. They are fairly straight and parallel to each other.

Immediately after quenching, tempering of steels was carried out at 673, 823 and 973 K. A typical TEM-bright micrograph of CrMo steel tempered at 973 K is given in Fig. 6a. As can be seen, the carbides are globularized and some rod shaped carbides are present. The dark-field micrograph for the carbide clearly show existence of cementite particles embedded in the ferrite matrix (Fig. 6b). The corresponding SAD pattern is given in Fig. 6c. The strong spots are from ferrite and the weaker ones from cementite. Indexing of SAD patterns confirmed that the carbides in this steel were orthorhombic cementite (Fig. 6d). The zone axis is [2 2 0] for the ferrite matrix, and [$\bar{1}$ 1 1] from the cementite, respectively. Thus, TEM bright- and dark-field micrographs as well as SAD pattern analysis of orientation relationship showed that the carbides were precipitated from ferrite matrix. Analysis by EDXS showed that the carbides are rich in iron together with some chromium (Fig. 7). This spectrum corresponds to the diagram of carbide stability for 2.25Cr–1Mo steel tempered at the same tempering temperature [26]. The Fe/Cr ratios reported in literature for this type of carbide vary between 1.6 and 24.0 in dependence on the type of the investigated steel and the tempering conditions [27, 28]. Low Fe/Cr ratio demonstrates the incorporation of chromium in the cementite already in the nucleation stage of this carbide.

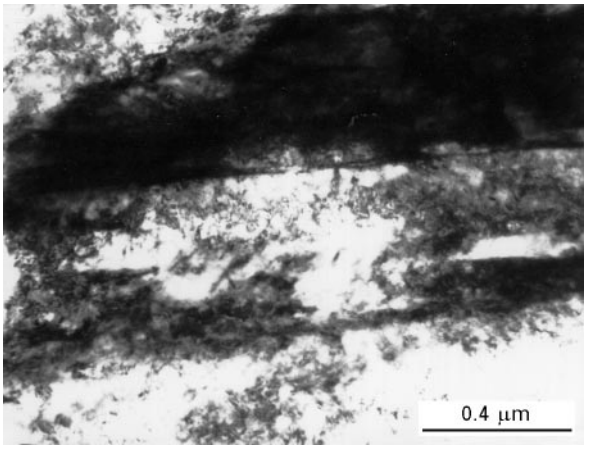

Figure 5 Transmission electron micrograph of low alloy CrMo steel austenized at 1123 K and quenched by flowing argon at the cooling rate of 30 K s^{-1}. Morphology of martensite is dislocated lath type.

The X-ray diffraction analysis showed that Cr steel contained only orthorhombic cementite, while CrMo steel contained the cementite and hexagonal Mo_2C particles (Fig. 8) in the ferrite matrix at the same tempering temperature (973 K). In addition to 0.11% Mo in Cr steel (Table I), the absence of Mo_2C in ferrite regions of Cr steel in the quenched and tempered condition can be explained on the basis of the fact that the driving force for the precipitation of the carbides is considerably lowered by the reduction in the Mo : C concentration ratio [8]. On the other side, for CrMo steel, Mo_2C particles may be nucleation at isolated dislocations within the ferrite as reported for Fe–C–Mo alloy in the temperature range from 748 to 898 K [29]. Baker and Nutting [6] observed also that at 823 K for water-quenched and tempered 2.25Cr–1Mo steels acicular Mo_2C carbides were precipitated.

The mechanical properties and the Vicker's hardness of Cr- and CrMo-steel in heat treated condition are summarized in Table III. The high mechanical properties of both steels may be attributed to interaction solid–solution hardening. This effect attributed to the strengthening due to the simultaneous presence in solution of substitutional and interstitial atoms with an affinity for each other (e.g. carbon and chromium or carbon and molybdenum). As a result of this strong attraction, atom pairs or atom clusters form and subsequently interact with dislocations to form atmospheres [30]. It is found that interaction solid-solution hardening effects have been attributed to carbon–molybdenum interactions in 2.25Cr–1Mo steel with a polygonal ferrite microstructure and to carbon–chromium interactions in the bainitic condition [31]. As can be seen (Table III), the mechanical properties decrease with increasing tempering temperature as a consequence of the increasing tempering temperature and microstructural changes. The decrease in strength is consistent with the work of Winter and Woodward [32], who showed that above 773 K the CrMo steel shows the spheroidization and coarsening of carbides, and the recovery and recrystallization of the cell structure (Fig. 6).

The CrMo steel compared with the Cr steel at the same tempered condition showed the higher strength but lower ductility (Table III). The reason for this is because of the microstructural features: finer prior austenite grain size (Fig. 1b), the substructure within the matrix (Fig. 6) and precipitate dispersion strengthening, primarily by Mo_2C (Fig. 8). The high affinity of molybdenum atoms for carbon atoms results in the formation of Mo–C clusters, which gradually grow and eventually transform into coherent M_2C precipitates. These precipitates introduce intense strain in the ferrite lattice leading to strengthening of steel. The strengthening of CrMo steel could be attributed to continued precipitation of Mo_2C carbides. Based on the available data on crystal lattice parameters, it is reasonable to conclude that the difference between the specific atomic volume of h.c.p. Mo_2C (17.7×10^3 nm^3) and of the b.c.c. ferrite (11.8×10^3 nm^3) surrounding

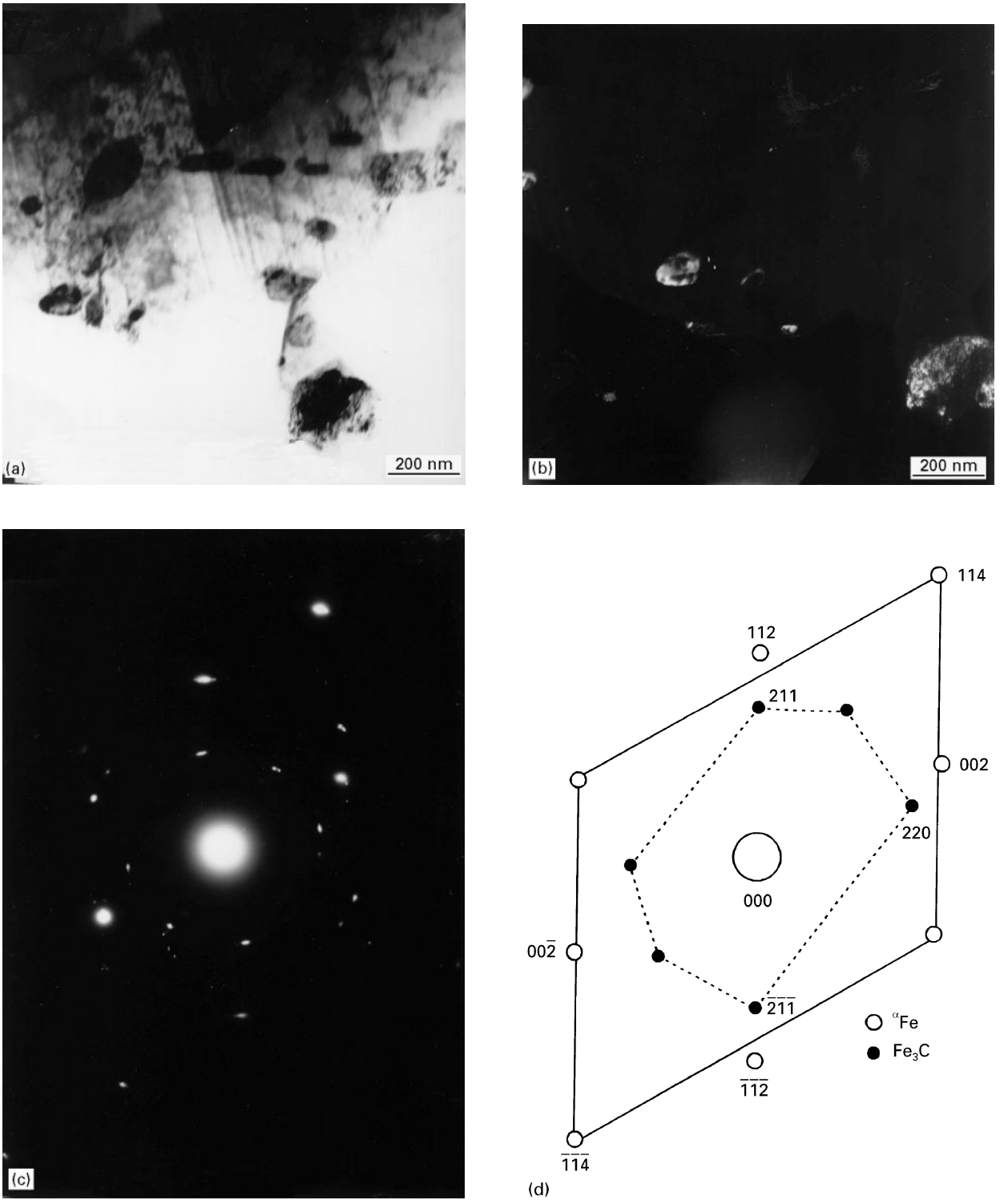

Figure 6 Transmission electron micrographs of low alloy CrMo steel austenized at 1123 K and tempered at 973 K. (a) Bright-field image, (b) dark-field image of cementite, (c) selected area diffraction pattern in (a) with the cementite orientation spot, (d) analysis of the SAD pattern in (c).

it, is very high, leading to elastic distortion of the host lattice and the precipitate. The coherent nature of the interface between Mo_2C and ferrite not only reduces the surface free energy, but also sets in coherency strain in the matrix, which in turn is responsible for the observed strengthening of CrMo steel. Similar observations of a uniform dispersion of such fine carbides contributing to significant strengthening in CrMo steels have been reported earlier [33].

3.3. Fractography analysis

It is well known that fractography directly represents the mechanisms involved in the fracture process and provides valuable informations concerning the cause of failure. The fracture surfaces of steels tempered at 673 K are shown in Fig. 9. The fracture surface of Cr steel consists of a mixed dimpled and quasi-cleavage failure (Fig. 9a), while the fracture mode of CrMo steel exhibited some dimpled fracture and a significant amount of intergranular fracture (Fig. 9b).

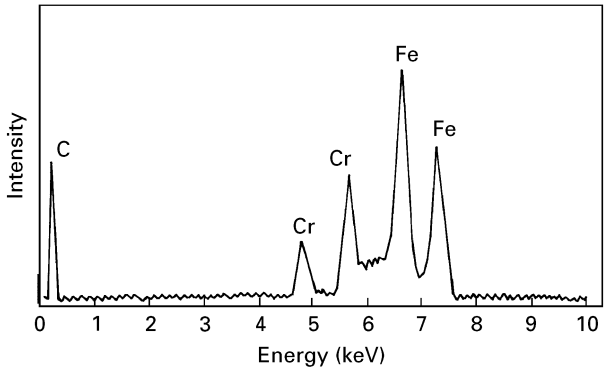

Figure 7 Energy dispersive X-ray spectrum of cementite shown on the bright-field image in Fig. 6a.

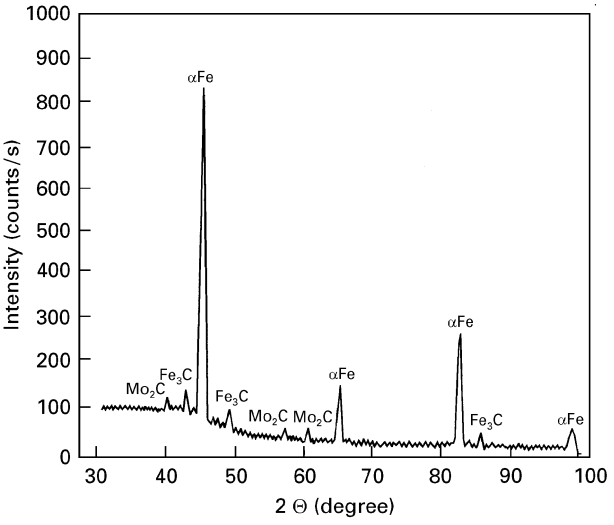

Figure 8 X-ray diffraction spectrum of low alloy CrMo steel tempered at 973 K.

TABLE III Mechanical properties of low alloy Cr and CrMo steel in quenched and tempered conditions

Steel	Heat treatment	Yield strength (MPa)	Tensile strength (MPa)	Reduction of Area (%)	Hardness ($H_{V_{30}}$)
Cr	Q: 1123 K/600 s	–	–	–	661
	Q: 1123 K/600 s + T: 673 K/2400 s	1410	1430	15	467
	Q: 1123 K/600 s + T: 823 K/2400 s	1012	1082	37	351
	Q: 1123 K/600 s + T: 973 K/2400 s	708	797	50	247
CrMo	Q: 1123 K/600 s	–	–	–	710
	Q: 1123 K/600 s + T: 673 K/2400 s	1670	1712	10	491
	Q: 1123 K/600 s + T: 823 K/2400 s	1265	1370	22	406
	Q: 1123 K/600 s + T: 973 K/2400 s	814	932	36	310

Q, quenching by argon; T, tempering in air.

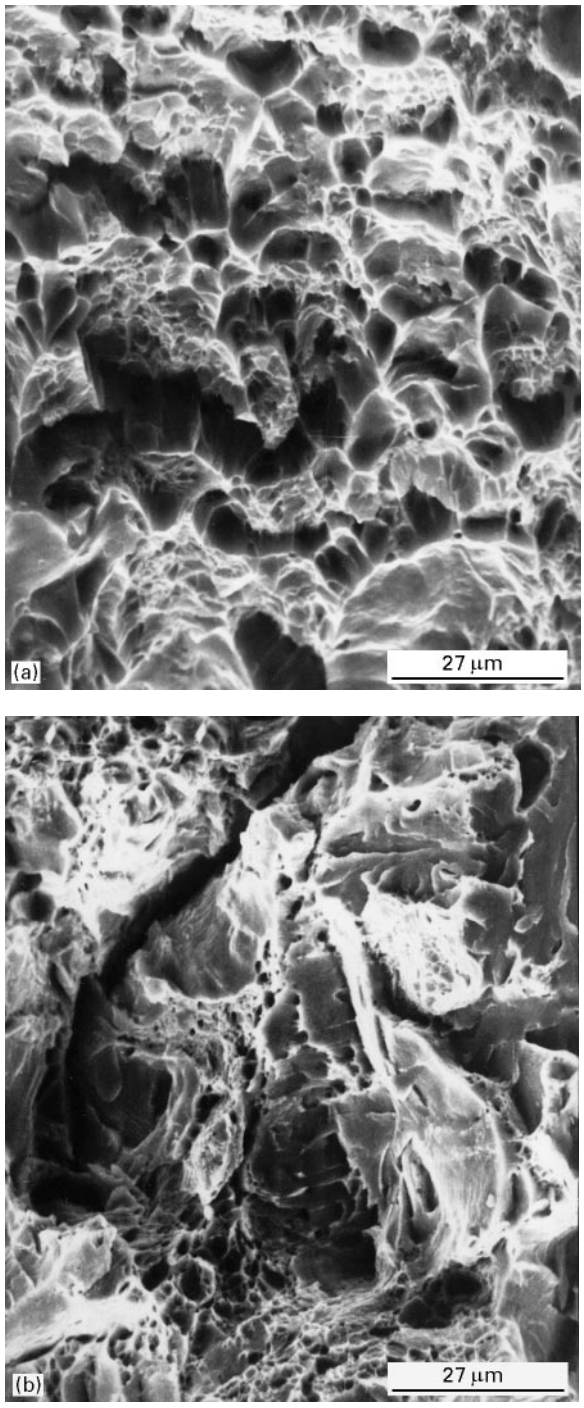

Figure 9 Scanning electron microscopy fractographs of low alloy Cr (a) and CrMo (b) steel tempered at 673 K.

The brittle intergranular fracture mode is thought to result from impurity-induced weaking at prior austenite grain boundaries as documented [34, 35]. In addition to this intergranular fracture there are also secondary cracking.

Fig. 10 shows typical fracture surfaces of steels tempered at 973 K. As can be seen, the fracture mode of steels is predominantly ductile with well-defined dimples. These fracture surfaces contained two sets of dimples: a set of large dimples that was initiated at MnS inclusion and a set of smaller ones, distributed between the larger dimples that was formed at submicrometre-sized carbides. The ductile fracture of steels was formed by the microvoid coalescence mechanism. The voids were formed around the large MnS inclusion

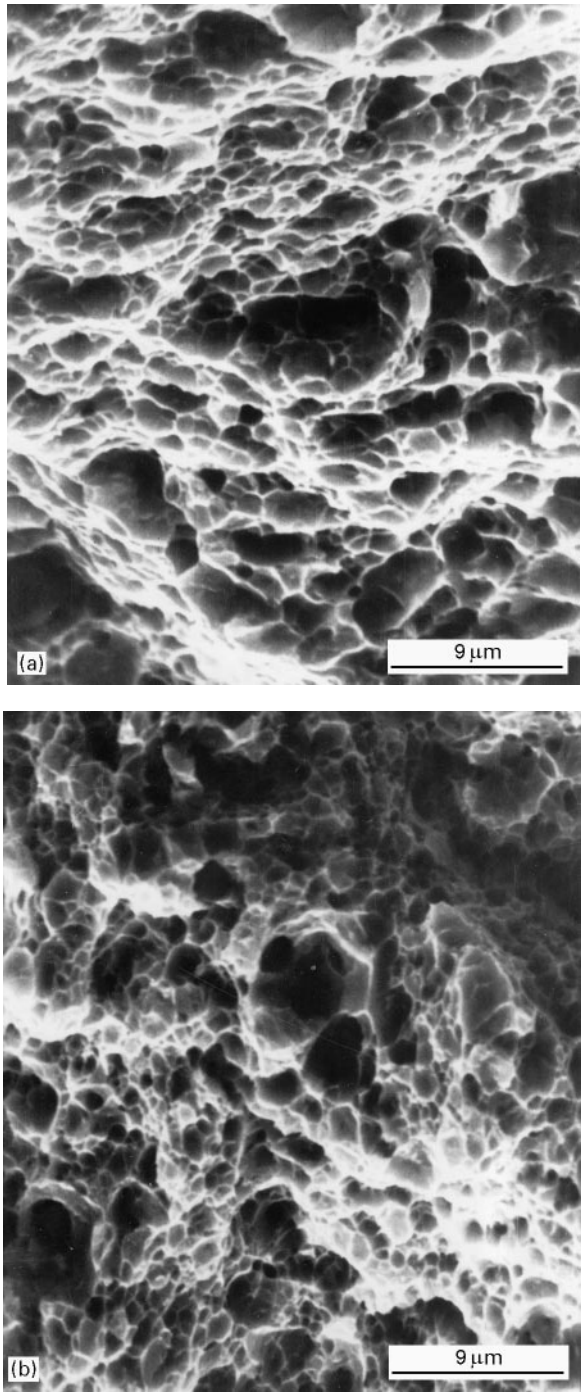

Figure 10 Scanning electron microscopy fractographs of low alloy Cr (a) and CrMo (b) steel tempered at 973 K.

first. As these voids grow, the deformation becomes localized into intense shear bands between the voids. The fracture occurs along these shear bands, and the fracture surface will contain large equiaxed voids. Since dispersion of carbides is present in the matrix (cementite and Mo_2C), the high strains within the shear bands also can cause microvoids to be formed at the carbide-matrix interfaces. Voids will be formed within the shear bands around these carbides, and fracture will occur.

4. Conclusions

The results of the investigation of low alloy Cr- and CrMo-steel can be summarized as follows:

1. The mechanical properties of steels in rolled condition resulted from the bainite microstructure obtained by the continuous cooling with finish temperature rolling of 1153 K.
2. Quenching of steels by flowing argon in the temperature range from 1123 to 573 K at the average cooling rate of $30\,K s^{-1}$ the martensite dislocated lath type with 2 vol% retained austenite was obtained.
3. Tempering of steels at 973 K was accompanied by the formation of subgrains as well as precipitation and spheroidization of carbide in the ferrite matrix.
4. After tempering at 973 K the Cr steel contains only orthorhombic cementite, while the CrMo steel contains the cementite and hexagonal Mo_2C particles. It was observed that the cementite precipitated from the ferrite matrix.
5. At the same tempering temperature, the CrMo steel shows higher strength but lower ductility as compared to the Cr steel. This is because of the finer prior austenite grains, substructure in the ferrite matrix and the precipitation dispersion strengthening, primarily by Mo_2C.
6. During the increase of the tempering temperature changes of morphology fracture surface were observed. Tempering at 973 K resulted in the ductile fracture by the microvoid coalescence mechanism.

References

1. P. J. GROBNER, D. L. SPONSELLER and D. E. DIESBURG, *Mater. Perf.* **14** (1975) 35.
2. N. GOPE, A. CHATTERJEE, T. MUKHERJEE and D. S. SARMA, *Metall. Trans.* **24A** (1993) 315.
3. P. J. NAYLOR, *ibid.* **10A** (1979) 861.
4. Y. TOMITA and K. OKABAYASHI, *ibid.* **17A** (1986) 1203.
5. B. UHRENIUS, in "Hardenability concepts with applications to steel", edited by D. V. Doane and J. S. Kirkaldy (AIME, Warrendale, 1978) p. 28.
6. R. G. BAKER and J. NUTTING, *J. Iron Steel Inst.* **192** (1959) 257.
7. M. C. MURPHY and G. D. BRANCH, *ibid.* **209** (1971) 546.
8. J. PILLING and N. RIDLEY, *Metall. Trans.* **13A** (1982) 557.
9. V. A. BIŠS and T. WADA, *ibid.* **16A** (1985) 109.
10. B. D. CRAIG, *Metall. Trans.* **13A** (1982) 23.
11. J. M. CHILTON and P. M. KELLY, *Acta Metall.* **16** (1968) 637.
12. Y. TOMITA and K. OKABAYASHI, *Metall Trans.* **18A** (1987) 115.
13. M. ENOMOTO, S. H. SONG, K. YAMADA, M. SHIMIZU and T. KUNIO, *J. Soc. Mech. Eng.* **40** (1974) 407.
14. S. WEISSMANN (ed.) "Search manual for selected powder diffraction data for metals and alloys", (JCPDS International center for Diffraction Data, Pennsylvania, Swarthmore, 1978).
15. M. GOJIĆ, A. PRELOŠČAN and M. MALINA, *Metalurgija* **30** (1991) 161.
16. B. C. CRAIG, *Metall. Trans.* **13A** (1982) 1099.
17. M. HILLERT, *ISIJ Int.* **35** (1995) 1134.
18. L. J. HABRAKEN and M. ECONOMOPOULOS, "Transformation and hardenability in steels" (Climax Molybdenum Company, Ann Arbor, MI, 1967) p. 69.
19. M. E. BUSH and P. M. KELLY, *Acta metall.* **19** (1971) 1363.
20. H. P. OFFER, J. F. COPELAND, J. L. YUEN and W. D. CHALLENGER, in "Effects of melting and processing variables on the mechanical properties of steels", edited by G. V. Smith (ASME, New York, NY, 1977) p. 195.
21. R. L. KLUEH and J. L. GRIFFITH, *J. Mater. Energy Syst.* **3** (1981) 26.

22. D. L. SPONSELLER, R. GARBER and T. B. COX, in Proceedings of the First International Conference on Current Solutions to Hydrogen Problems in Steels, Washington DC, November 1982, edited by C. G. Interrante and G. M. Pressouyre (ASM, Metals Park, Ohio, 1982) p. 200.
23. R. KASPAR, U. LOTTER and C. BIEGUS, *Steel Res.* **65** (1994) 242.
24. M. SARIKAYA, B. G. STEINBERG and G. THOMAS, *Metall. Trans.* **13A** (1982) 2227.
25. B. V. N. RAO and G. THOMAS, *ibid.* **11A** (1980) 441.
26. J. YU, *ibid.* **20A** (1989) 1561.
27. R. D. GRIFFIN, R. A. DODD, G. L. KULCINSKI and D. S. GELLES, *ibid.* **21A** (1990) 1853.
28. J. JANOVEC, A. VYROSTKOVA and A. HOLY, *J. Mater. Sci.* **27** (1992) 6564.
29. H. TSUBAKINO and H. I. AARONSON, *Metall. Trans.* **18A** (1987) 2047.
30. J. B. BAIRD and A. JAMIESON, *J. Iron Steel Inst.* (*London*) **210** (1972) 847.
31. R. L. KLUEH, *Mater. Sci. Engng* **35** (1978) 239.
32. P. L. WINTER and R. L. WOODWARD, *Metall. Trans.* **17A** (1986) 307.
33. S. SAROJA, M. VIJAYALAKSHIMI and V. S. RAGHUNATHAN, *J. Mater. Sci.* **27** (1992) 2389.
34. R. O. RITCHIE, *Metall. Trans.* **8A** (1977) 1131.
35. S. YU and C. J. McMAHON Jr., *ibid.* **11A** (1980) 277.

Received 30 July 1996
and accepted 5 August 1997